


## Article

# Sequential Design of Decentralized Robust Controllers for Strongly Interconnected Inverter-Based Distributed Generation Systems: A Comparative Study versus Independent Design

Milad Shojaee<sup>1</sup> and S. Mohsen Azizi<sup>1,2,\*</sup> 

<sup>1</sup> Department of Electrical and Computer Engineering, New Jersey Institute of Technology, Newark, NJ 07102, USA; ms2892@njit.edu

<sup>2</sup> School of Applied Engineering and Technology, New Jersey Institute of Technology, Newark, NJ 07102, USA

\* Correspondence: azizi@njit.edu

**Abstract:** Internal oscillations among multiple generation systems in low-voltage stand-alone nanogrids and small-scale microgrids can cause instability in the entire generation system. This issue becomes worse when the coupling strength between the generation systems increases, which is a result of a shorter distance between them and a smaller reactance to resistance ratio. Previous approaches, which were based on the independent control design and considered the coupling effect as disturbances, may fail to tackle this issue when the two generation systems become strongly coupled. Therefore, in this paper a novel method is proposed to handle this coupling effect by designing robust decentralized controllers in a sequential manner to address the problem of voltage and frequency control in a nanogrid. This proposed sequential design is a general technique that is applicable to multiple inverter-based generation systems in a nanogrid or small-scale microgrid. For the ease of demonstration, in this paper the case of two interconnected inverters with LC output filters is studied. Two robust decentralized controllers are designed for the two inverter systems by using the  $\mu$ -synthesis technique. The sequential design takes into account the interconnection line between the two inverters. Moreover, the controllers are designed to be robust against all the parameter variations in the system including the LC filter and interconnection line parameters. The simulation results demonstrate the superior performance of the proposed controller over the independently-designed controllers for the case of two generation systems that are highly coupled due to the short distance between them. Moreover, the proposed controller is shown to be robust against the LC filter and interconnection line parameter uncertainties as compared to the sequentially-designed linear quadratic Gaussian controllers.

**Keywords:** coupled systems;  $\mu$ -synthesis; nanogrid; robust controller; sequential design; inverter; uncertainty



**Citation:** Shojaee, M.; Azizi, S.M. Sequential Design of Decentralized Robust Controllers for Strongly Interconnected Inverter-Based Distributed Generation Systems: A Comparative Study versus Independent Design. *Energies* **2022**, *15*, 8995. <https://doi.org/10.3390/en15238995>

Academic Editors: Gibran David Agundis Tinajero, Yajuan Guan and Juan C. Vasquez

Received: 21 October 2022

Accepted: 24 November 2022

Published: 28 November 2022

**Publisher's Note:** MDPI stays neutral with regard to jurisdictional claims in published maps and institutional affiliations.



**Copyright:** © 2022 by the authors. Licensee MDPI, Basel, Switzerland. This article is an open access article distributed under the terms and conditions of the Creative Commons Attribution (CC BY) license (<https://creativecommons.org/licenses/by/4.0/>).

## 1. Introduction

Distorted voltage and current waveforms in low-voltage (LV) nanogrids (NGs) and small-scale microgrids (SSMGs) are crucial problems, as they lead to low energy efficiency and power quality deterioration [1]. Such distortions can provoke resonance in the system, which may lead to instability [2]. This problem is of more importance in LV standalone NGs and SSMGs, where multiple generation systems are connected together within short distances, and the coupling strength between them is increased.

Employed as interfaces between renewable energy sources such as wind turbines and photovoltaic units and the utility grid, inverters are one of the most indispensable units in NGs and SSMGs due to the global penetration of renewable energy sources [3]. Total harmonic distortion of the inverter output current can be decreased by using LC filters. Such passive filters are commonly used in solar systems to minimize the amplitude of



harmonics, thus enhancing the power quality [4]. Nonetheless, such passive filters give rise to undesired resonances and bring about more challenges for the design of controllers [5].

Aside from the abovementioned challenges, with the proliferation of NGs and SSMGs, the distances between generation systems have considerably decreased, which in turn has decreased the  $X/R$  ratio and increased the dynamic coupling strength between them [6]. In addition, using power electronic-based generation systems in such NGs and SSMGs decreases the total inertia of the system, which can cause fluctuations due to disturbances and the strengthened coupling between the inverter systems through the interconnection line [7]. In conventional generation systems, synchronous generators are employed as the main source of power, which have higher inertia due to the presence of the mechanical interfaces. The low inertia of inverters as well as the strengthened coupling between them introduce instability into the system, which needs to be addressed by designing advanced controllers. To this end, robust controllers should be designed for strongly coupled distributed generators to tackle the problem of instability.

The control of inverter-based interconnected generation systems has been addressed by several studies in the literature. In [8], a nonlinear droop control scheme was used to enhance the power-frequency performance and to tackle the transient active power sharing issues in parallel NGs. In [9], a hierarchical control scheme was presented for a multi-bus NG consisting of PV generations, battery storage systems, and loads. The power flow was regulated to ensure the technical feasibility of the obtained setpoints. A new droop control strategy for NGs in the islanded mode was presented in [10], where the proposed controller ameliorated the dynamics of the power electronic interfaces in NGs. In [11,12], a fuzzy-based control scheme was proposed to tackle the weak power-sharing performance issue of a droop control system due to the network impedance. However, the case of  $X/R \ll 1$ , which is equivalent to shorter interconnection distances, was not considered in their analyses. In [6], an  $H_\infty$  control of a system with two interconnected voltage source converters (VSCs) was presented to damp the low-frequency oscillations. The effect of the network dynamics on the stability of SSMGs was investigated in [13], where a particular model-order reduction method was used to systematically account for the network dynamics.

In [14], a decentralized voltage and frequency control of off-grid AC SSMGs based on an interconnection and damping assignment passivity-based control was proposed. An adaptive control of frequency and voltage using distributed cooperative control and adaptive neural networks was presented in [15] for inverter-based distributed multi-microgrids. In [16], a two-level distributed control scheme was presented to bring together the distributed energy resources in low-voltage SSMGs, where the interconnections were considered to be resistive. Another similar study was presented in [17], where a distributed control strategy was introduced to regulate the voltage and power of interconnected SSMGs. In [18], an efficient reduced-order model of inverter-based SSMGs was presented, whose structure was similar to the quasistationary model and included the effects of network dynamics. The issue of a low  $X/R$  ratio in the low-voltage SSMGs was investigated in [19], where the impact of the interconnection line and droop controllers were assessed. In [20], the issue of SSMG instability was addressed by introducing a systematic scheme to determine the proper size of the virtual impedance, thus improving the stability of the droop control. A model-free centralized control scheme was proposed in [21] to coordinate inverters in a dispatchable SSMG, such that it operated as a single-controllable resistor. In [3], a decentralized robust control strategy based on the  $\mu$ -synthesis technique was presented to control the voltage of an inverter in an isolated SSMG.

One of the main problems that has not been fully addressed in the aforementioned studies is the variation in the interconnection coupling strength caused by the distance changes between the generation systems. In other words, as the distance between generation systems decreases, the interconnection strength between them increases to the point where the entire system becomes unstable. This issue is not of high concern for the grid-tied generation systems in which the power system is stabilized by the grid. However, in



standalone NGs, where the distances between different distributed generation systems are shorter, the effect of the coupling strength on frequency fluctuations becomes more crucial. Even though some studies have considered the low interconnection distances between the generation systems, there has been no analysis and guarantee of the robustness against the changes in the system parameters. Considering the fact that islanded NGs and SSMGs are becoming more frequent [22,23], designing robust controllers that can take into account this coupling effect as well as other parameter uncertainties can significantly improve the issue of instability in such cases.

The goal of this study is to propose a novel robust control scheme, which considers the effect of coupling interconnections within the control design process. This control strategy is referred to as the sequential design of decentralized robust controllers. By designing the controllers in a sequential way, the robustness of the entire system against the variations in coupling strength as well as the LC filter parameters are improved considerably. Therefore, the main contributions of this study are summarized as follows:

1. Sequentially designing decentralized controllers for strongly coupled inverter-based generation systems in a nanogrid without communication links.
2. Ensuring the robustness of the decentralized controllers against the variations in all the parameters of the inverter-based generation system, while attenuated the resonance frequency of LC filters.
3. Conducting simulations to verify the superior performance of the proposed control system as compared to the independently-designed decentralized controllers as a benchmark.
4. Conducting simulations to show the superior performance of the proposed control system in terms of the robustness against the LC filter and interconnection line parameter variations as compared to linear quadratic Gaussian (LQG) controllers as a benchmark.

The rest of the paper is summarized as follows. In Section 2, the dynamical model of the two interconnected inverter-based distributed generation systems is presented. The system parameter variations and structured uncertainties are presented in Section 3. The proposed sequential decentralized control design is provided in Section 4. The simulation results and discussions are presented in Section 5. Finally, the conclusion of the paper is given in Section 6.

## 2. The Model of Interconnected Inverters in a Nanogrid

The investigated model in this study is demonstrated in Figure 1, where two inverters are connected by an interconnection line, for which both the inductive and resistive properties are considered. Such inverters are connected to renewable-based generation systems, such as wind turbines or photovoltaic panels. As illustrated in Figures 1 and 2, the inverters are connected to the energy storage systems, which are in turn charged by the energy from the renewable generation sources. The renewable generation systems have their own control systems that are decoupled from the control systems in the inverters, which is why they are not considered in this study (for more details, the reader is referred to [24]). The focus of this paper is to design decentralized robust controllers to regulate the voltages of the loads for the case of a short interconnection line between the two inverters. Figure 2 demonstrates a VSC combined with an LC filter for each one of the generation units. The objective of the decentralized controllers is to make the load voltage,  $v_{load}$ , follow a sinusoidal reference signal,  $v_{ref}$ , in the presence of a strong coupling between the two subsystems (inverters), the parameter uncertainties of the LC filter, and undesired disturbances in the load. It should be noted that the design of the LC filters is outside the scope of this work and can be found in [25,26].



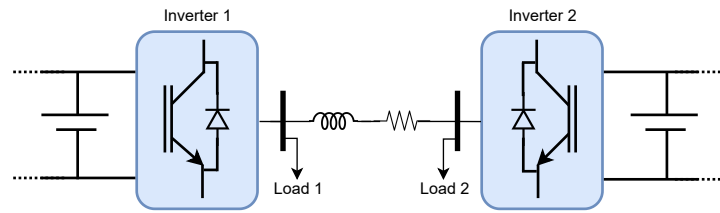


Figure 1. Interconnected inverters.

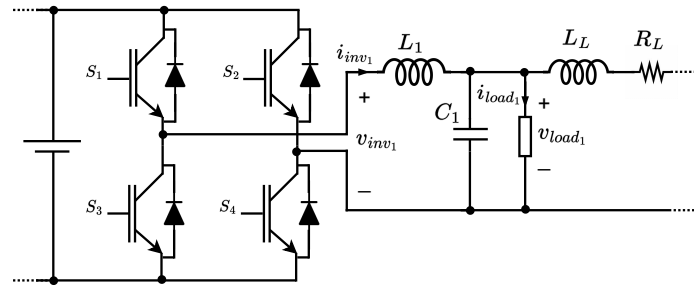


Figure 2. The circuit of a VSC with an LC filter connected to the load and interconnection line.

Based on the circuit illustrated in Figure 2, the corresponding open-loop dynamic equations of the system are as follows:

$$\begin{aligned}
 i_{inv1} &= G_{inv1}(v_{inv1} - v_{load1}) \\
 G_{inv1} &:= \frac{1}{L_1 s} \\
 v_{load1} &= G_{vc1}[i_{inv1} - i_{load1} - G_L(v_{load1} - v_{load2})] \\
 G_{vc1} &:= \frac{1}{C_1 s} \\
 G_L &:= \frac{1}{L_L s + R_L}
 \end{aligned} \tag{1}$$

The same set of equations can be obtained from the second subsystem (inverter). Finally, based on the dynamical equations in (1), the closed-loop block diagram of the two interconnected inverters is shown in Figure 3, where  $K_1$  and  $K_2$  represent the decentralized controller transfer functions, and  $M_{inv1}$  and  $M_{inv2}$  represent the inverter gains.

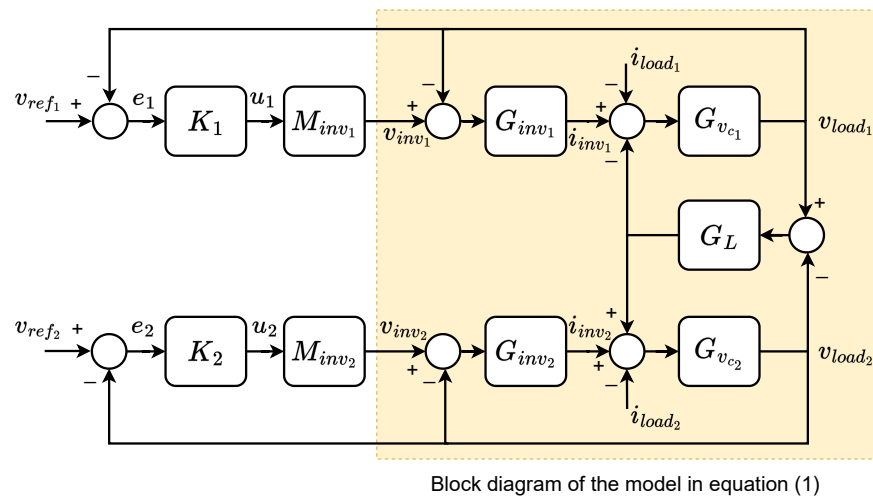


Figure 3. Closed-loop block diagram of the interconnected inverters with LC filters and interconnection line dynamics. The open-loop dynamic equations in (1) are highlighted by a yellow box.



### 3. Parameter Variations of the System and Structured Uncertainties

The uncertain parameters of the inverter model are the LC filter components and the interconnection line resistance and inductance parameters. In the  $\mu$ -synthesis framework, the range of the model parameter variations is the major design criterion, which is modeled by using multiplicative uncertainties as follows:

$$x = \bar{x}(1 + \mathcal{E}_x \delta_x), \quad (2)$$

where  $x$  and  $\bar{x}$  represent the uncertain and nominal parameter values, respectively, " $\mathcal{E}_x$ " amounts to the maximum percentage deviation of the parameter  $x$  from its nominal value, and " $\delta_x$ " pertains to the corresponding normalized uncertainty variable, such that  $|\delta_x| < 1$ .

By placing the multiplicative uncertainties defined in (2) into the associated transfer functions in (1) and using the upper linear fractional transformation (LFT) operator [3], the following uncertain transfer functions are obtained for the subsystem  $i$  ( $i = 1, 2$ ):

$$G_{inv_i}(s) = F_u(\bar{G}_{inv_i}(s), \delta_{L_i}) \quad (3)$$

$$\bar{G}_{inv_i}(s) \triangleq \frac{1}{\bar{L}_i s} \begin{bmatrix} -\bar{L}_i \mathcal{E}_{L_i} s & 1 \\ -\bar{L}_i \mathcal{E}_{L_i} s & 1 \end{bmatrix}$$

$$G_{v_{ci}}(s) = F_u(\bar{G}_{v_{ci}}(s), \delta_{C_i}) \quad (4)$$

$$\bar{G}_{v_{ci}}(s) \triangleq \frac{1}{\bar{C}_i s} \begin{bmatrix} -\bar{C}_i \mathcal{E}_{C_i} s & 1 \\ -\bar{C}_i \mathcal{E}_{C_i} s & 1 \end{bmatrix}$$

$$G_L(s) = F_u(\bar{G}_L(s), \begin{bmatrix} \delta_{L_L} \\ \delta_{R_L} \end{bmatrix}) \quad (5)$$

$$\bar{G}_L(s) \triangleq \frac{1}{\bar{L}_L s + \bar{R}_L} \begin{bmatrix} -\bar{L}_L \mathcal{E}_{L_L} s & -\bar{R}_L \mathcal{E}_{R_L} & 1 \\ -\bar{L}_L \mathcal{E}_{L_L} s & -\bar{R}_L \mathcal{E}_{R_L} & 1 \end{bmatrix}$$

where  $\bar{G}_{inv_i}(s)$ ,  $\bar{G}_{v_{ci}}(s)$ , and  $\bar{G}_L(s)$  represent the nominal transfer functions of their corresponding transfer functions, and  $F_u(\cdot, \cdot)$  is the LFT operator. The same transfer functions can be obtained for the parameters of the second inverter.

Figure 3 is extended into Figure 4 by using the aforementioned LFT models of uncertain parameters and corresponding transfer functions in Equation (1). As shown in the extended block diagram in Figure 4, the original transfer functions are replaced by the corresponding upper LFTs.

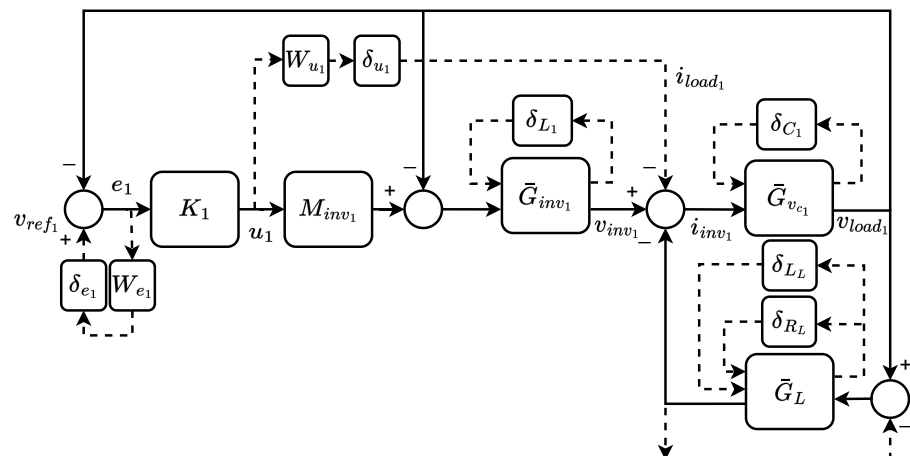


Figure 4. Extended block diagram of the first subsystem in Figure 3.



As seen in Figure 4,  $e_i$  ( $i = 1, 2$ ) is defined to be the voltage tracking error. The controller is required to satisfy the following constraints:

$$T_{e_i}(s)W_{e_i}(s) < \frac{1}{\delta_{e_i}} \quad (6)$$

$$T_{u_i}(s)W_{u_i}(s) < \frac{1}{\delta_{u_i}} \quad (7)$$

where  $T_{e_i}(s)$  and  $T_{u_i}(s)$  are the transfer functions from  $v_{ref_i}$  to  $e_i$  and  $i_{load_i}$  to  $u_i$ , respectively, and  $\delta_{e_i}$  and  $\delta_{u_i}$  ( $i = 1, 2$ ) determine the tightness of the above constraints. Moreover, the choice of the two performance weight functions,  $W_{e_i}$  and  $W_{u_i}$  allocated to the variables  $e_i$  and  $u_i$ , respectively, affects the time response of the closed-loop system. Their parameters are selected such that the best time response of the system is achieved. The following choices were made in this study for the abovementioned transfer functions and parameters:

$$W_{u_i}(s) = 10^{-3} \quad (8)$$

$$\delta_{e_i} = \delta_{u_i} = 1$$

$$W_{e_i}(s) = \frac{100}{s(0.001s + 1)} \prod_{j=1,3,5,7} \frac{s^2 + 1000s + j^2\omega_g^2}{s^2 + s + j^2\omega_g^2},$$

where  $\omega_g = 2\pi f$  (rad/s), and  $f = 60$  (Hz).

In the next section, the extended model in Figure 4 is used to design sequential decentralized robust controllers in the framework of  $\mu$ -synthesis.

#### 4. Sequential Decentralized $\mu$ -Synthesis Design

The  $\mu$ -synthesis structure in the form of  $\Delta/Q/K$  (uncertainty/nominal system/controller) is obtained from the extended system illustrated in Figure 4. This structure is demonstrated in Figure 5.

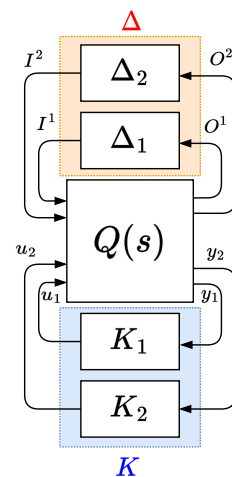


**Figure 5.** The  $\mu$ -synthesis structure of the two interconnected inverters.

In this regard, the uncertainty matrix  $\Delta$  of the system has the following block-diagonal structure, which consists of the uncertain parameters of the model:

$$\Delta = \text{diag}(\Delta_1, \Delta_2) \quad (9)$$

$$\Delta_i = \text{diag}(\Delta_i^a, \Delta_i^b), i = 1, 2$$

$$\Delta_i^a = \text{diag}([\delta_{L_i} \quad \delta_{R_i}], \delta_{L_i}, \delta_{C_i})$$

$$\Delta_i^b = \text{diag}(\delta_{e_i}, \delta_{u_i}),$$



where the operator “diag” represents the block-diagonal concatenation of its arguments.

All of the nominal transfer functions of the extended model are combined together to define  $Q(s)$  as demonstrated in Figure 6, where the operators  $I^i(\cdot)$  and  $O^i(\cdot)$  represent the input and output of the nominal transfer function  $Q(s)$  associated with the subsystem (inverter) # $i$  ( $i = 1, 2$ ), respectively, and are defined as follows:

$$I^i(Q) = \begin{bmatrix} I(\bar{G}_{inv_i}) \\ I(\bar{G}_{v_{ci}}) \\ I_1(\bar{G}_{L_i}) \\ I_2(\bar{G}_{L_i}) \\ i_{load_i} \\ v_{ref_i} \end{bmatrix}, O^i(Q) = \begin{bmatrix} O(\bar{G}_{inv_i}) \\ O(\bar{G}_{v_{ci}}) \\ O(\bar{G}_{L_i}) \\ W_{u_i}u_i \\ W_{e_i}e_i \end{bmatrix} \quad (10)$$

where the operators  $I(\cdot)$  and  $O(\cdot)$  represent the input and output of their arguments, respectively, and the operator  $I_i(\cdot)$  ( $i = 1, 2$ ) represents the  $i$ th input of its argument.

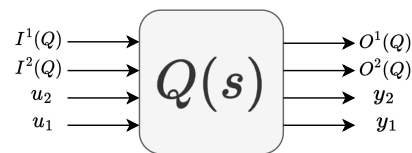


Figure 6. Inputs and outputs of the nominal system  $Q(s)$ .

The decentralized robust controllers  $K_1(s)$  and  $K_2(s)$  are designed based on the following Laplace-domain robust control condition [27]:

$$\mu_{\Delta}(F_L(Q(s), K(s))) < 1 \quad (11)$$

$$K(s) \triangleq \text{diag}(K_1(s), K_2(s)),$$

where  $F_L(\cdot, \cdot)$  represents the lower LFT of its arguments, and “ $\mu(\cdot)$ ” denotes the  $\mu$ -norm and is defined in (12) as follows:

$$\mu_{\Delta}(X) \triangleq \frac{1}{\min_{\Delta \in \Delta} \{\bar{\sigma}(\Delta) : \det(I - X\Delta) = 0\}}, \quad (12)$$

where  $\Delta$  and  $\bar{\sigma}$  represent the uncertainty block diagonal matrix, defined in (9), and the largest singular value operator, respectively. If there is no  $\Delta \in \Delta$  such that  $\det(I - X\Delta) = 0$ , then  $\mu_{\Delta}(X)$  is equal to zero.

Because of the block-diagonal form of the controller  $K(s)$ , the classical  $\mu$ -synthesis design cannot be carried out. One way to tackle this issue is to execute the  $\mu$ -synthesis design process in two steps for  $K_1(s)$  and  $K_2(s)$ , sequentially. In other words, the first controller  $K_1(s)$  is designed for the transfer function  $Q(s)$  that is attached to the matrix  $\Delta_1$  by an upper LFT, while the second controller  $K_2(s)$  and the uncertainty matrix  $\Delta_2$  are left open as shown in Figure 7a. After the first controller is designed, it is connected to the system  $Q(s)$  by a lower LFT. Then, considering both uncertainty matrices  $\Delta_1$  and  $\Delta_2$  as shown in Figure 7b, the second controller is designed for the whole system. The details of this procedure are summarized in the following five steps:

Step 1. While the connections corresponding to the controller  $K_2(s)$  and the uncertainty matrix  $\Delta_2$  are left open, the controller  $K_1(s)$  is designed by using the  $D$ - $K$  iteration algorithm in such a way that the following Laplace-domain robust criterion holds:

$$\mu_{\Delta_1}(F_L(Q_1(s), K_1(s))) < 1, \quad (13)$$







**Table 1.** The values of the system parameters used in simulations.

First inverter	$M_{inv_1} = 1$ , $L_1 = 3.0$ (mH), $C_1 = 2.0$ ( $\mu$ F), $L_{load_1} = 1.0$ (H), $R_{load_1} = 630$ ( $\Omega$ )
Second inverter	$M_{inv_2} = 1$ , $L_2 = 2.8$ (mH), $C_2 = 2.2$ ( $\mu$ F), $L_{load_2} = 1.2$ (H), $R_{load_2} = 632$ ( $\Omega$ )
Interconnection line	$R_L = 0.642$ ( $\Omega$ /km), $L_L = 2.2 \times 10^{-4}$ (H/km) [28]

### 5.1. Real-Time Simulation Using OPAL-RT

The MATLAB/SIMULINK R2019a software was used to simulate the closed-loop control system, and the OPAL-RT (OP5700) real-time simulator was used to conduct the real-time simulations. OPAL-RT has two platforms for its computations, namely CPU and FPGA. The CPU specifications are Intel Xeon E5, 8 Cores, 3.2 (GHz), and 20 (MB) cache memory, which is used to simulate slow dynamics such as mechanical, grid, and control systems with the simulation step size of 10 ( $\mu$ s)–100 ( $\mu$ s). The FPGA platform is used for fast dynamics with the simulation step size of 100 (ns)–1 ( $\mu$ s) for power electronics in which the high frequency gate signals of the power transistors are simulated and generated by the FPGA. OPAL-RT is a powerful tool for the hardware-in-the-loop (HIL) simulations, which include both the steady-state and transient responses, providing a complete and comprehensive solution for the HIL simulation. The applications of OPAL-RT are in the realm of power systems, power electronics, aerospace, and automotive sectors [29]. The simulations in OPAL-RT were run in real-time due to the fact that all three stages in Figure 8 including the measurements, computations, and commands were executed in a time window shorter than the simulation step size specified for the application. In other words, the controller needed to receive the feedback measurements, execute the control algorithm, and generate the command signal within the simulation step size. The simulation step size for the slow dynamics of the closed-loop control system, which are used by the CPU, as well as the fast dynamics of the power electronics, which are used by the FPGA, were calculated as follows:

- The bandwidth of the closed-loop control system was 6.66 (kHz). The sampling frequency was set to ten times faster, i.e.,  $6.66 \text{ (kHz)} \times 10 = 66.6 \text{ (kHz)}$ , which was equivalent to the simulation step size of 15 ( $\mu$ s).
- The switching frequency of the power electronic unit was 1 (MHz). The sampling frequency in the FPGA platform was set to ten times faster, i.e.,  $1 \text{ (MHz)} \times 10 = 10 \text{ (MHz)}$ , which was equivalent to the simulation step size of 100 (ns).

The real-time OPAL-RT simulator includes a FPGA platform that can accurately represent inverters and their switching mechanism by using hardware description language (HDL). The OPAL-RT and its FPGA unit have been verified to be able to provide a very accurate simulation of inverters [30,31]. To this end, the FPGA provides the following advantages:

- The computation time within each time step is independent of the size of the system due to the parallel nature of the FPGAs.
- Overruns do not happen while the model is running.
- The simulation step size is very small, in the order of 100 (ns).
- The corrective algorithms for the inter-simulation time-step switching events can be eliminated without jeopardizing the accuracy or the numerical stability.



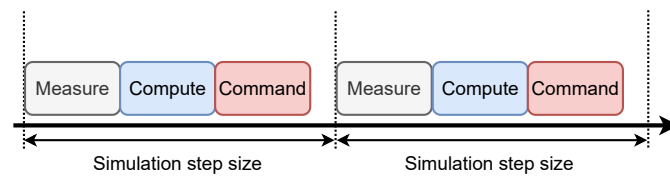


**Figure 8.** Real-time simulation timing diagram.

### 5.2. Robust Control Conditions

Figures 9 and 10 illustrate the robust control conditions in Equations (13) and (14), respectively, for the sequential design of the decentralized robust controllers. The  $\mu$ -norm in both steps of the design process was less than one, which indicates that Equations (13) and (14) and thus Equation (11) were satisfied.

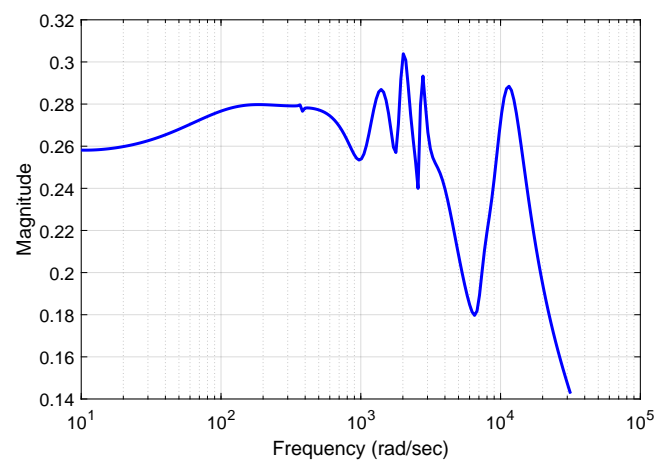


**Figure 9.** Robust control condition for the sequential design in Equation (13) (Step 1 of the proposed 5-step design procedure).

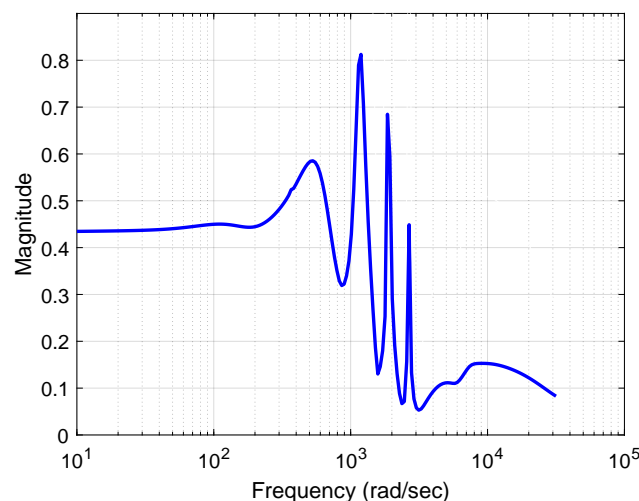


**Figure 10.** Robust control condition for the sequential design in Equation (14) (Step 3 of the proposed 5-step design procedure).

### 5.3. Time Response Performance

The interconnection line parameters are proportional to the distance between the two inverters, which play an important role in the coupling strength between the two inverters and the stability of the entire system. All the simulation results for the proposed



sequentially-designed decentralized controllers were compared with the independently-designed ones in which the effect of the interconnection line is considered as an external disturbance. The details of the independent design of the decentralized robust controllers can be found in [3]. The following two case studies were considered in order to compare the two control designs in terms of their performances with respect to the interconnection line distance between the two inverters.

- The first case study was for the distance of 1 (km). Figures 11 and 12 demonstrate the time response of the load and reference voltages for the sequentially and independently-designed controllers, respectively. Both controllers had acceptable performances in tracking the reference voltage when the distance between the inverters was 1 (km).
- The second case study was for the distance of 200 (m). The time responses of the load and reference voltages for the sequentially and independently-designed controllers are shown in Figures 13 and 14, respectively. In this case, the interconnection strength between the inverters was larger as compared to the first case study, which in turn led to the instability of the independently-designed control system. The control system designed by the sequential method remained stable with an acceptable performance, while the one designed by the independent scheme started to have unstable oscillations around  $t = 0.01$  (s).

It was concluded that the distance of 200 (m) between the two generation systems was the borderline of stability for the independently-designed decentralized controllers. The main reason is that the independent design of decentralized controllers does not consider the coupling dynamics (through the interconnection line) between the two inverters. On the other hand, the sequential design takes the complete dynamics of the interconnection line into account in order to design the decentralized controllers. The proposed sequential control design technique is applicable to any small networks of inverters such as NGs and SSMGs.

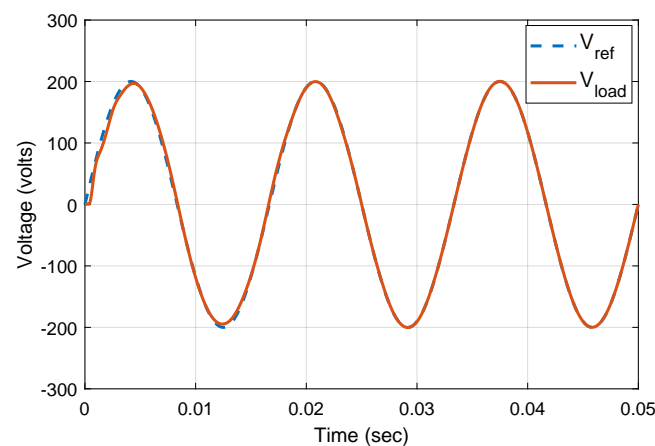


**Figure 11.** Time response of the sequentially-designed decentralized controllers for 1 (km) distance between the inverters.



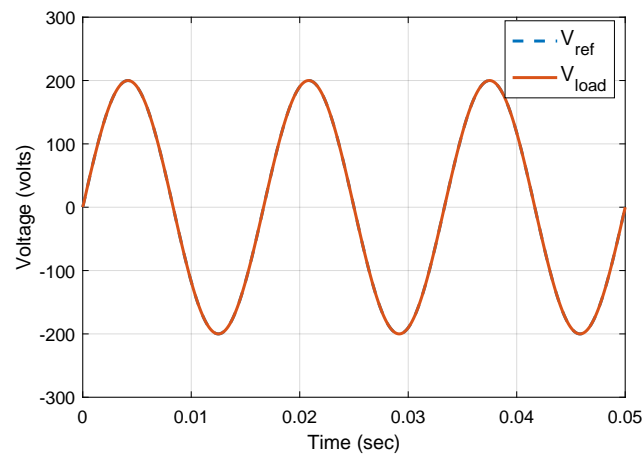


**Figure 12.** Time response of the independently-designed decentralized controllers for 1 (km) distance between the inverters.

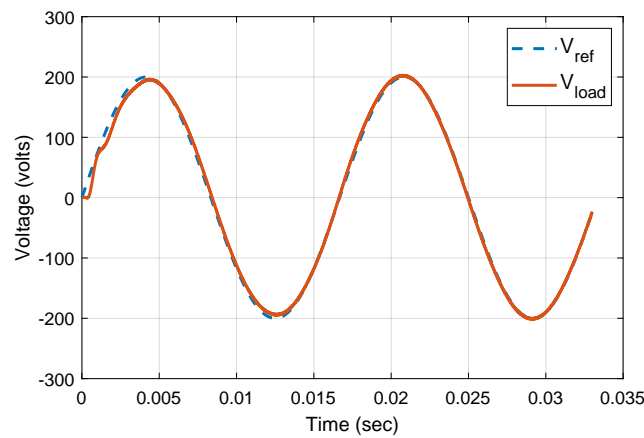


**Figure 13.** Time response of the sequentially-designed decentralized controllers for 200 (m) distance between the inverters.

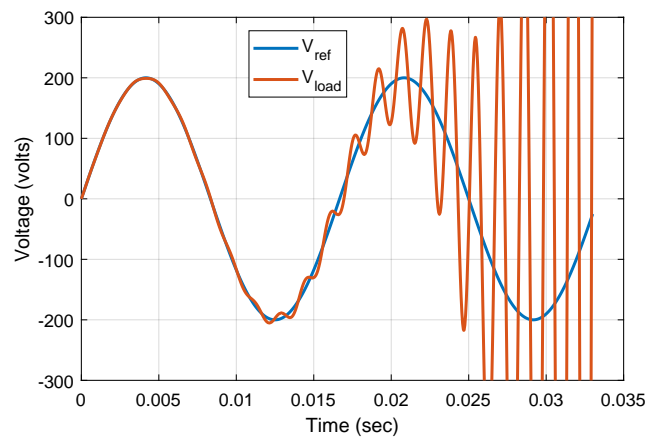


**Figure 14.** Time response of the independently-designed decentralized controllers for 200 (m) distance between the inverters.

#### 5.4. Robustness Analysis

Due to the variations in the parameters of the LC filters, the closed-loop control system was expected to be robust against them. According to [30], the variations in the LC values are within  $\pm 10\%$  of their nominal values. In this study, the variations were considered to



be  $\pm 20\%$ , which provided more margin. The interconnection line parameters were also taken as uncertain parameters. Since this work is in the context of nanogrids and small-scale microgrids, the interconnection line parameter values are volatile due to the location changes made by users that will impact the lengths and parameter values of the interconnection lines. Moreover, the cables and wires in the scale of nanogrids are influenced by the transmitted electrical signals of other devices, which consequently impact their impedance values [31]. Since the independent design of the decentralized controllers showed poor performance when the interconnection coupling increased, the robust performance of the proposed control scheme was compared with that of the sequentially-designed decentralized LQG controllers. The reason to choose LQG control design as a benchmark is due to its optimal control performance against uncertainty [32]. Figures 15 and 16 demonstrate the time response of both the proposed control and LQG control schemes for  $\pm 20\%$  parameter variations of LC filters as well as the interconnection line parameters, respectively. As observed, the proposed control design had better robustness as compared to the benchmark due to the consideration of the parameter uncertainties by the control design process.

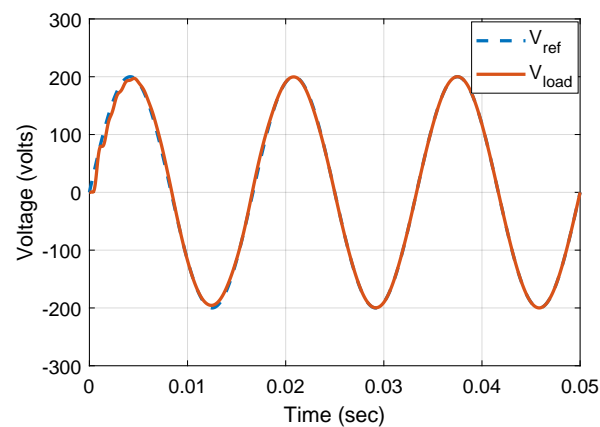


**Figure 15.** Time response of the sequentially-designed decentralized controllers for 500 (m) distance between the inverters and  $\pm 20\%$  variations in the parameters of the LC filters and the interconnection line.

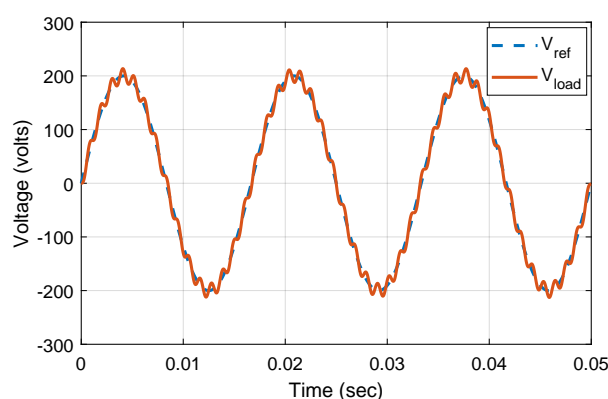


**Figure 16.** Time response of the sequentially-designed decentralized LQG controllers for 500 (m) distance between the inverters and  $\pm 20\%$  variations in the parameters of the LC filters and the interconnection line.

### 5.5. Resonance Analysis

As mentioned before, the LC filters give rise to undesired resonance frequencies in the system, which make the control design more challenging. However, the decentralized robust controllers proposed in this work were able to attenuate this resonance frequency



significantly as depicted in Figure 17, which illustrates the open-loop and closed-loop Bode diagrams of the generation system 1.

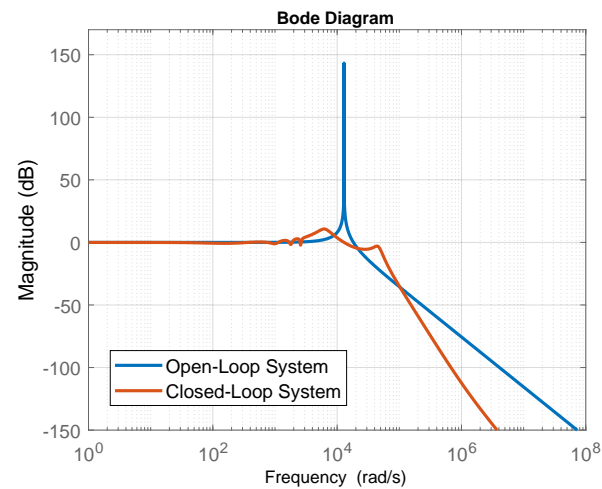


**Figure 17.** Open-loop and closed-loop frequency responses of the generation system 1 with the LC filter resonance frequency.

## 6. Conclusions

In this paper, a decentralized robust control scheme based on sequential design was proposed to tackle the voltage control and regulation problem for two inverter-based generation systems, which are strongly coupled. The generation systems are connected together through an interconnection line consisting of inductive and resistive components. The proposed robust controller included two local controllers for the two generation systems, which were designed sequentially by using the  $\mu$ -synthesis technique. As the controllers had a block-diagonal structure, there was no communication link between them. Furthermore,  $\pm 20\%$  variations were considered for all the uncertain parameters of the nanogrid, which were modeled by structured uncertainties. These uncertainties were taken into account in the process of designing the robust decentralized controllers. The simulation results demonstrated that the decentralized controllers satisfied the Laplace-domain condition of robust control. Moreover, under strong interconnection between the generation systems, the decentralized controllers designed sequentially outperformed the decentralized controllers designed independently. The main reason is that the sequential design considered the impact of coupling among the generation systems in the design process of the controllers, whereas the independent design treated them as disturbances. Furthermore, the superior robust performance of the proposed controllers over the LQG controllers was demonstrated. It was also verified that the sequentially-designed decentralized controllers successfully attenuated the resonance frequency. This study suggests that as the distances among generation systems in a standalone nanogrid become shorter, the independently-designed controllers result in instability, while the proposed sequentially-designed controllers performed well.

**Author Contributions:** Conceptualization, S.M.A.; methodology, M.S.; software, M.S.; validation, M.S.; data curation, M.S.; writing—original draft preparation, M.S.; writing—review and editing, M.S. and S.M.A.; visualization, M.S.; supervision, S.M.A.; funding acquisition, S.M.A. All authors have read and agreed to the published version of the manuscript.

**Funding:** This research was partially supported by the National Science Foundation (Advanced Technological Education program) under Grant No. 1902442.

**Data Availability Statement:** Not applicable.

**Conflicts of Interest:** The authors declare no conflict of interest.



## Nomenclature

$\delta_x$	Normalized uncertainty variable for the parameter $x$
$\mathcal{E}_x$	Maximum percentage deviation of the parameter $x$
$\mu$	$\mu$ -norm operator
$\omega_g$	Frequency of the generation systems
$e_i$	Error signal of the generation system $i$ ( $i = 1, 2$ )
$F_u$	Upper linear fractional transformation (LFT) operator
$G_L$	Transfer function of the interconnection line between the two inverters
$i_{inv_i}$	Inverter current of the generation system $i$ ( $i = 1, 2$ )
$i_{load_i}$	Load current of the generation system $i$ ( $i = 1, 2$ )
$K_i$	Decentralized controller's transfer function of the generation system $i$ ( $i = 1, 2$ )
$M_i$	Inverter gain of the generation system $i$ ( $i = 1, 2$ )
$u_i$	Control signal of the generation system $i$ ( $i = 1, 2$ )
$v_{inv_i}$	Inverter voltage of the generation system $i$ ( $i = 1, 2$ )
$v_{load_i}$	Load voltage of the generation system $i$ ( $i = 1, 2$ )
$v_{ref_i}$	Reference voltage of the generation system $i$ ( $i = 1, 2$ )
$W_{e_i}$	Error performance weight function for the generation system $i$ ( $i = 1, 2$ )
$W_{u_i}$	Input performance weight function for the generation system $i$ ( $i = 1, 2$ )

## References

- Hogan, D.J.; Gonzalez-Espin, F.J.; Hayes, J.G.; Lightbody, G.; Foley, R. An adaptive digital-control scheme for improved active power filtering under distorted grid conditions. *IEEE Trans. Ind. Electron.* **2017**, *65*, 988–999. [\[CrossRef\]](#)
- Argüello, A.; Torquato, R.; Freitas, W.; Padilha-Feltrin, A. A graphical method to assess component overload due to harmonic resonances in wind parks. *IEEE Trans. Power Deliv.* **2020**, *36*, 1819–1828. [\[CrossRef\]](#)
- Azizi, S.M.; Khajehoddin, S.A. Robust inverter control design in islanded microgrids using  $\mu$ -synthesis. In Proceedings of the 2016 IEEE Energy Conversion Congress and Exposition (ECCE), Milwaukee, WI, USA, 18–22 September 2016; pp. 1–5.
- Adak, S. Harmonics Mitigation of Stand-Alone Photovoltaic System Using LC Passive Filter. *J. Electr. Eng. Technol.* **2021**, *16*, 2389–2396. [\[CrossRef\]](#)
- Twining, E.; Holmes, D.G. Grid current regulation of a three-phase voltage source inverter with an LCL input filter. *IEEE Trans. Power Electron.* **2003**, *18*, 888–895. [\[CrossRef\]](#)
- Eskandari, M.; Savkin, A.V. A Critical Aspect of Dynamic Stability in Autonomous Microgrids: Interaction of Droop Controllers through the Power Network. *IEEE Trans. Ind. Inform.* **2021**, *18*, 3159–3170. [\[CrossRef\]](#)
- Ratnam, K.S.; Palanisamy, K.; Yang, G. Future low-inertia power systems: Requirements, issues, and solutions-A review. *Renew. Sustain. Energy Rev.* **2020**, *124*, 109773. [\[CrossRef\]](#)
- Berzoy, A.; Salazar, A.; Khalizheli, F.; Restrepo, C.; Velni, J.M. Non-linear Droop Control of Parallel Split-phase Inverters for Residential Nanogrids. In Proceedings of the 2019 IEEE Applied Power Electronics Conference and Exposition (APEC), Anaheim, CA, USA, 17–21 March 2019; pp. 1150–1156. [\[CrossRef\]](#)
- González-Romera, E.; Roncero-Clemente, C.; Barrero-González, F.; Milanés-Montero, M.I.; Romero-Cadaval, E. A Comprehensive Control Strategy for Multibus Nanogrids With Power Exchange Between Prosumers. *IEEE Access* **2021**, *9*, 104281–104293. [\[CrossRef\]](#)
- Kaviri, S.M.; Hajebrahimi, H.; Poorali, B.; Pahlevani, M.; Jain, P.K.; Bakhshai, A. A Supervisory Control System for Nanogrids Operating in the Stand-Alone Mode. *IEEE Trans. Power Electron.* **2021**, *36*, 2914–2931. [\[CrossRef\]](#)
- Eskandari, M.; Li, L.; Moradi, M.H. Improving power sharing in islanded networked microgrids using fuzzy-based consensus control. *Sustain. Energy Grids Netw.* **2018**, *16*, 259–269. [\[CrossRef\]](#)
- Eskandari, M.; Li, L.; Moradi, M.H.; Wang, F.; Blaabjerg, F. A control system for stable operation of autonomous networked microgrids. *IEEE Trans. Power Deliv.* **2019**, *35*, 1633–1647. [\[CrossRef\]](#)
- Vorobev, P.; Huang, P.H.; Al Hosani, M.; Kirtley, J.L.; Turitsyn, K. A framework for development of universal rules for microgrids stability and control. In Proceedings of the IEEE 56th Annual Conference on Decision and Control (CDC), Melbourne, Australia, 12–15 December 2017; pp. 5125–5130.
- Strehle, F.; Malan, A.J.; Krebs, S.; Hohmann, S. A port-hamiltonian approach to plug-and-play voltage and frequency control in islanded inverter-based ac microgrids. In Proceedings of the IEEE 58th Conference on Decision and Control (CDC), Nice, France, 11–13 December 2019; pp. 4648–4655.
- Amoateng, D.O.; Al Hosani, M.; Elmoursi, M.S.; Turitsyn, K.; Kirtley, J.L. Adaptive voltage and frequency control of islanded multi-microgrids. *IEEE Trans. Power Syst.* **2017**, *33*, 4454–4465. [\[CrossRef\]](#)
- Golsorkhi, M.S.; Shafiee, Q.; Lu, D.D.C.; Guerrero, J.M. Distributed control of low-voltage resistive AC microgrids. *IEEE Trans. Energy Convers.* **2018**, *34*, 573–584. [\[CrossRef\]](#)
- Golsorkhi, M.S.; Hill, D.J.; Karshenas, H.R. Distributed voltage control and power management of networked microgrids. *IEEE J. Emerg. Sel. Top. Power Electron.* **2017**, *6*, 1892–1902. [\[CrossRef\]](#)



18. Vorobev, P.; Huang, P.H.; Al Hosani, M.; Kirtley, J.L.; Turitsyn, K. High-fidelity model order reduction for microgrids stability assessment. *IEEE Trans. Power Syst.* **2017**, *33*, 874–887. [\[CrossRef\]](#)
19. Eskandari, M.; Savkin, A.V. Interaction of droop controllers through complex power network in microgrids. In Proceedings of the IEEE 18th International Conference on Industrial Informatics (INDIN), Warwick, UK, 20–23 July 2020; pp. 311–314.
20. Huang, P.H.; Vorobev, P.; Al Hosani, M.; Kirtley, J.L.; Turitsyn, K. Plug-and-play compliant control for inverter-based microgrids. *IEEE Trans. Power Syst.* **2019**, *34*, 2901–2913. [\[CrossRef\]](#)
21. dos Santos Alonso, A.M.; Brandao, D.I.; Tedeschi, E.; Marafão, F.P. Resistive shaping of interconnected low-voltage microgrids operating under distorted voltages. *IEEE Trans. Ind. Electron.* **2021**, *69*, 9075–9086. [\[CrossRef\]](#)
22. Xu, Y.; Yi, Z. Chapter 3—Optimal distributed secondary control for an islanded microgrid. In *Distributed Control Methods and Cyber Security Issues in Microgrids*; Academic Press: Cambridge, MA, USA, 2020; pp. 59–81.
23. Shojaei, M.; Mohammadi Shakiba, F.; Azizi, S.M. Decentralized Model-Predictive Control of a Coupled Wind Turbine and Diesel Engine Generator System. *Energies* **2022**, *15*, 3349. [\[CrossRef\]](#)
24. Amouzegar Ashtiani, N.; Azizi, S.M.; Khajehoddin, S.A. Robust Control Design for High-Power Density PV Converters in Weak Grids. *IEEE Trans. Control. Syst. Technol.* **2019**, *27*, 2361–2373. [\[CrossRef\]](#)
25. Habetler, T.; Naik, R.; Nondahl, T. Design and implementation of an inverter output LC filter used for  $dv/dt$  reduction. *IEEE Trans. Power Electron.* **2002**, *17*, 327–331. [\[CrossRef\]](#)
26. Mishra, P.; Maheshwari, R. Design, Analysis, and Impacts of Sinusoidal LC Filter on Pulsewidth Modulated Inverter Fed-Induction Motor Drive. *IEEE Trans. Ind. Electron.* **2020**, *67*, 2678–2688. [\[CrossRef\]](#)
27. Liu, K.Z.; Yao, Y. *Robust Control: Theory and Applications*; John Wiley & Sons: Hoboken, NJ, USA, 2016.
28. Rocabert, J.; Luna, A.; Blaabjerg, F.; Rodriguez, P. Control of power converters in AC microgrids. *IEEE Trans. Power Electron.* **2012**, *27*, 4734–4749. [\[CrossRef\]](#)
29. Opal-rt Technologies. Available online: <https://www.opal-rt.com/> (accessed on 27 November 2022).
30. Nguyen, H.T.; Kim, E.K.; Kim, I.P.; Choi, H.H.; Jung, J.W. Model predictive control with modulated optimal vector for a three-phase inverter with an LC filter. *IEEE Trans. Power Electron.* **2017**, *33*, 2690–2703. [\[CrossRef\]](#)
31. Leuchter, J.; Dong, Q.H.; Boril, J.; Blasch, E. Electromagnetic immunity of aircraft wireless and cables from electromagnetic interferences. In Proceedings of the IEEE/AIAA 36th Digital Avionics Systems Conference (DASC), St. Petersburg, FL, USA, 17–21 September 2017; pp. 1–6.
32. Ueda, J.; Gallagher, W.; Moualeu, A.; Shinohara, M.; Feigh, K. Adaptive human-robot physical interaction for robot coworkers. In *Human Modelling for Bio-Inspired Robotics*; Academic Press: Cambridge, MA, USA, 2017; pp. 297–333.